COMMUNICATION

Factors Driving the Ni/Cu Cooperative Asymmetric Propargylation of Aldimine Esters†

Received 00th January 20xx,
Accepted 00th January 20xx

DOI: 10.1039/x0xx00000x

Giuseppe Sciortino ,[a] and Feliu Maseras [a]

The factors driving the Ni^0(binap)/Cu^I(phospherrox) cooperative asymmetric propargylation of aldimine esters are unveiled through DFT calculations. The system is fully explored accounting for conformational complexity and aggregation steps. The activation of the substrates proceeds independently, while the intercatalyst communication occurs both through indirect cooperativity, exchanging the non-innocent $MeCO_2^-$, and through direct cooperation in the stereoselective C-C coupling driven by intercatalyst interactions.

Multimetallic systems are expanding the frontiers of modern organometallic catalysis toward new synthetic challenges.[1-5] The synergistic activation of distinct co-substrates or functionalities avoids harsh conditions, and can lead to a safer chemistry, with waste reduction and atom economy.[3] However, a complete control of the synergy between the catalytic partners has not been reached yet. There remain open questions on intimate mechanism, redox compatibility and competition between catalytic cycles.[6] Computational chemistry, particularly density functional theory (DFT) is a promising tool for the mechanistic clarification of cooperative processes,[7-18] but due to the large dimension and conformational complexity of these multicomponent systems, deep mechanistic studies are still scarce.[19, 20,21] The few available publications show a picture with a wide diversity of mechanisms, from those where a supramolecular bimetallic complex acts as an effective catalyst throughout all the steps; to those where different monometallic complexes activate different substrates and only interact at the end. In this context, we became intrigued by reports of a series of bimetallic catalytic systems based on transition metal complexes of bidentate chiral phosphines. The cooperativity of Cu/Ir, Rh/Pd, Pd/Cu, Cu/Na and Ni/Cu couples led to the asymmetric synthesis in mild condition of chiral homoallylic amines,[22] indole derivatives,[23] γ-butyrolactones,[24] O-propargyl hydroxylamines,[25] and α-quaternary propargylated amino ester.[26, 27, 28, 29, 30] We will examine here this latter case, the synthesis of α-quaternary propargylated amino ester by asymmetric propargylation of aldimine esters using propargylic carbonates, reported by Guo and co-workers.[26] The bimetallic system consists of Ni^0 and Cu^I complexes containing the chiral bidentate binap and phosferrox type ligands (Scheme 1).[‡] The reaction proceeds at room temperature reaching up to 94% of yield and >99% of enantiomeric excess (ee). The cooperative details and stereodetermining factors of this innovative system could not be fully characterized in the experimental report. In particular, questions arise regarding: i) a full mechanistic picture of the transformation; ii) the identity of the base assisting the aldiminic C-H activation; iii) the factors governing the stereocontrol of the transformation; and iv) the level of Ni/Cu cooperation along the reaction pathway.

Here we report a mechanistic study on this system at a B3LYP-D3 theory level in a DCM continuum model.[§] The real catalytic system was introduced in the calculation as [Ni^0(**L_1**)(COD)] ((*R*)-**L_1**, Ar=Ph) and [Cu^I(**L_2**)$(MeCN)_2$]$^+$, ((*R,S,Sp*)-**L_2**, R=Ph). **L_2**, with R=Ph, was chosen instead of the phosphine with R=4-MeC_6H_4 in order to reduce the dimension of the full system. In fact, both ligands shared the same ee with quite similar reaction yields, 70% and 80%, respectively.

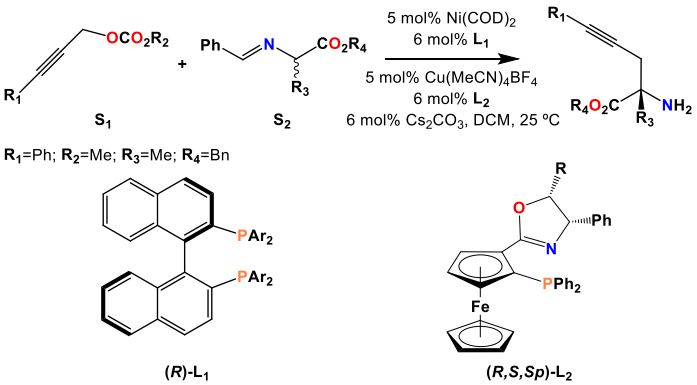

Scheme 1. Representation of the chiral phosphine ligands, reaction conditions for the asymmetric propargylic alkylation of aldimine esters.

[a] *Institute of Chemical Research of Catalonia (ICIQ), The Barcelona Institute of Science and Technology, Av. Països Catalans 16, 43007 Tarragona, Spain.*

†Electronic Supplementary Information (ESI) available: Full computational details; Energy profiles; Cartesian coordinates.

We selected methyl (3-phenylprop-2-yn-1-yl) carbonate, **S₁** (**R₁**=Ph, **R₂**=Me), and benzyl 2-(benzylideneamino) propanoate, **S₂** (**R₃**=Me, **R₄**=Bn) as model substrates because they are the simplest examples producing 99% ee.[26]

The formation of the Ni^0(**L₁**) and Cu^{II}(**L₂**) complexes is assumed since they are independently synthesized in different reaction flasks.[26] The coordination of **S₁** and **S₂** to both co-catalysts was evaluated, obtaining the lower ΔG_{DCM} of formation for [Ni^0(**L₁**)(**S₁**)] and [Cu^I(**L₂**)(**S₂**)]$^+$ in agreement with the experimental outcome (see Table S1). Then me moved to evaluate the isomeric and conformational landscape of the single co-catalysts. [Ni^0(**L₁**)(**S₁**)] is a square planar complex, as expected for Ni^0, in which the **S₁** substrate displays an η^2 coordination mode (Fig. 1a). An alternative **S₁**-κO coordination was found to have an energy more than 35 kcal·mol^{-1} higher, and was thus discarded (see Table S2). [Cu^I(**L₂**)(**S₂**)]$^+$ is characterized by an **S₁**-κ^2N,O coordination in a distorted seesaw arrangement, displaying two possible coordination isomers, *SS*-15-A and *SS*-15-C with similar stability (labels SS-15 correspond to "seesaw 1,5", A/C correspond to clockwise/anticlockwise orientations, Fig. 1b). Our results are in line with those obtained by Hou and co-workers for analogous chiral Cu^I(phosphorrox)/imino esters systems.[31] For *SS*-15-A an additional low energy isomer with **S₁**-κ^2N,O' is possible (Fig. S1). All isomers were taken into account along the mechanistic analysis.

The reaction mechanism was first analysed considering the independent activation of both substrates, Fig. 2. On the nickel side, after the η^2 coordination of the propargylic carbonate **S₁**, an oxidative addition (OA) through a low barrier of 13.2 kcal·mol^{-1} involving the cleavage of the C(sp^2)-O bond leads to the propargyl-Ni Intermediate **II**, -1.0 kcal·mol^{-1} below the reactants. Intermediate **II** is a Ni^{II} square pyramidal complex with the η^3 coordination of the electrophilic propargyl moiety and a slight axial interaction (Ni···O 2.460 Å) of the leaving methyl carbonate (Fig. 2).

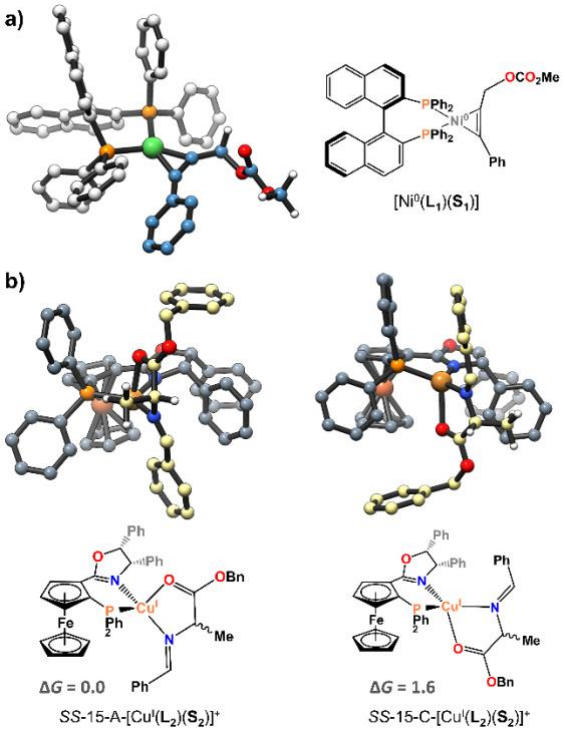

Fig. 1. Optimized geometries for activated co-catalysts [Ni^0(**L₁**)(**S₁**)] and [Cu^I(**L₂**)(**S₂**)]$^+$. Hydrogen atoms are omitted for clarity.

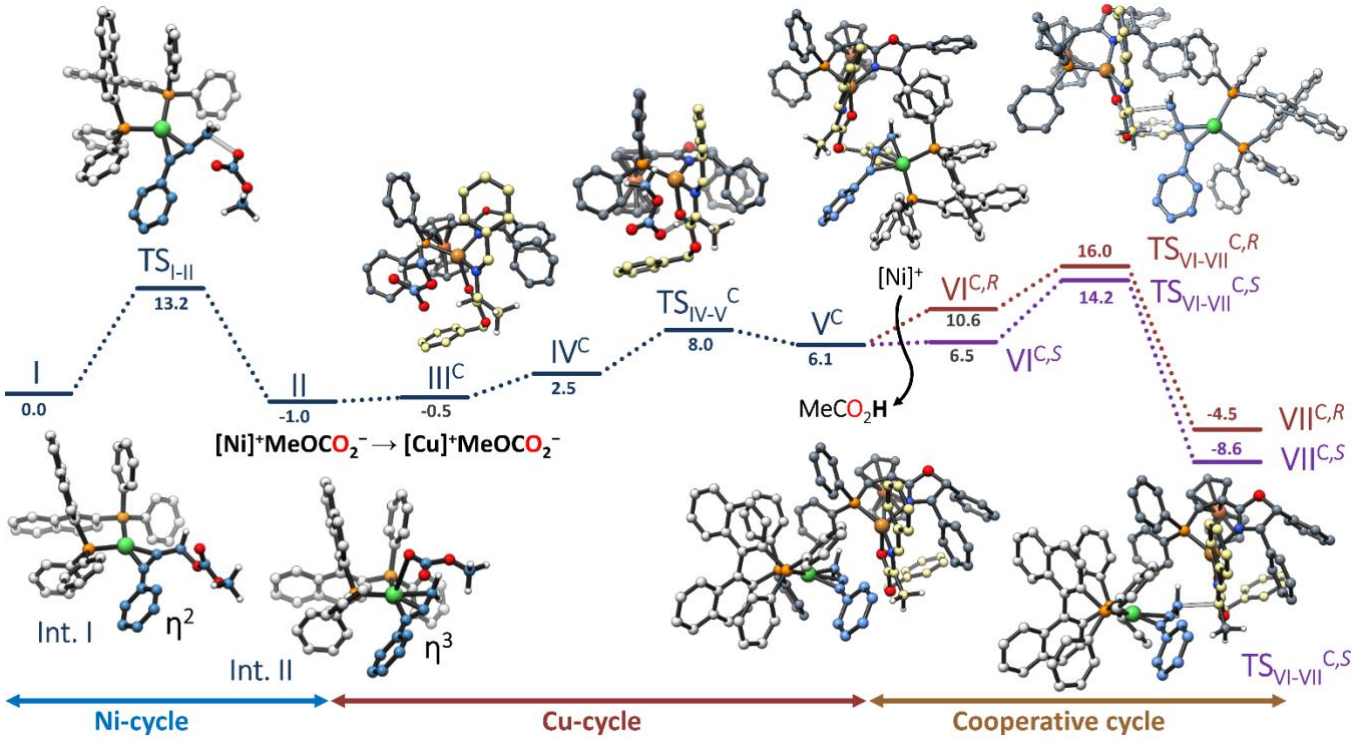

Fig. 2. DFT computed mechanism (B3LYP-D3 in CH_2Cl_2) for the propargylation with **S₁** of the aldimine ester **S₂** considering the independent activation of the substrates. The superindexes "C" refer to the clockwise orientation in the *SS*-15-C isomers. The numbers are relative Gibbs energies in kcal mol^{-1}, taking as zero-energy the separated co-catalysts and substrates **S₁** and **S₂**. A complete overview of all the intermediates is given in Fig. S3 of the ESI.

Intermediate **II** can in principle evolve following two different pathways: i) isomerization into intermediate **II'**, at 3.8 kcal·mol^{-1}, in which the η^1-**S$_1$** propargylic moiety and $MeOCO_2^-$ coordinates in the equatorial plane and subsequent decarboxylation and MeO^- release; or ii) direct release of the $MeOCO_2^-$ fragment retaining the η^3-coordination mode of the propargylic moiety. On the one hand, for the decarboxylation to proceed the system need to overcome an energy barrier of 5.6 kcal·mol^{-1} (**TS$_{II'-III'}$**) yielding [Ni^{II}(**L$_1$**)(propargyl)(MeO)] at 3.7 kcal·mol^{-1} (intermediate **III'**). The relese of MeO^- is a highly exergonic step requiring about 20 kcal·mol^{-1}. On the other hand, the direct release of $MeOCO_2^-$ is feasible process requiring 3.4 kcal·mol^{-1} (see Fig. S2). Concerning the copper cycle, the formation of the nucleophile entails a base-assisted aldiminic C(*sp*^{2})-H activation over [Cu^I(**L$_2$**)(**S$_2$**)]$^+$. Among the anions present in solution, $MeOCO_2^-$, generated on the Ni cycle, is the most promising candidate for the C-H activation, as it can be easily exchanged between both catalysts (ΔG_{DCM} = 0.5 kcal·mol^{-1}) (see Fig. S2). The role of $MeOCO_2^-$ as base is in agreement with the reported yield increment (from 59% to 80%) in presence of Cs_2CO_3, which presumably, acts as a base for the proton abstraction at the beginning of the reaction. We then investigated the efficiency of the two possible O-groups of methyl carbonate toward the base-assisted C-H activation (see Fig. S4). $MeOCO_2^-$ mediated proton abstraction was computed for all anti- and clockwise seesaw isomers obtaining a preference by more than 4 kcal·mol^{-1} for the *SS*-15-C isomer **IV^C** (see Fig. S5). **TS$_{IV-V}^C$** brings to the prochiral nucleophile **V^C** falling at 6.1 kcal·mol^{-1} (Fig. 2). The following step, after the approach of both co-catalysts in intermediate **VI^C**, consists in the asymmetric coupling of the activated moieties by cooperative C-C bond formation. The subsequent transition state **TS$_{VI-VII}^C$**, has the highest barrier for the process, which leads to an associated energy span of 15.2 kcal·mol^{-1}, consistent with a process at room temperature. This step also defines the enantioselectivity of the reaction. The prochiral intermediate **VI^C** can, in principle, approach the Ni electrophilic moiety offering either the *Si* or *Re* faces of the imino ester plane, leading to the amino ester with *R* or *S* configuration of the α carbon, respectively. Both possibilities were explored obtaining two TSs differing in the relative orientation of the co-catalysts (see Fig. 3). The most favourable TS is the one leading to the *S* enantiomer as observed experimentally. The pro-*(R)* TS was found 1.8 kcal mol^{-1} above. From these values the calculated enantiomeric excess is 92%, which is in line with the experimental value of 99%.

The factors governing this selectivity were investigated by activation strain model and NCI analysis (Table S2 and Fig. 3). Non-covalent interaction (NCI) analysis[32] shows that the intermolecular NCIs between either the chiral co-catalyst or the activated co-substrates moieties contribute to stabilize the pro-*(S)* transition state. As shown in Fig. 3, in the pro-*(S)* TS: i) the phenyl substituents of the phosphine centers of both chiral co-catalysts generate a larger π–π interaction surface than in the pro-*(R)* (3.9 vs 5.0 Å, **1** and **1'** in Fig. 3); and ii) more extended CH–π interactions are observed between both activated co-substrates (3.0 vs 3.7 Å, **2** and **2'** in Fig. 3) thus leading to a lower energy barrier.

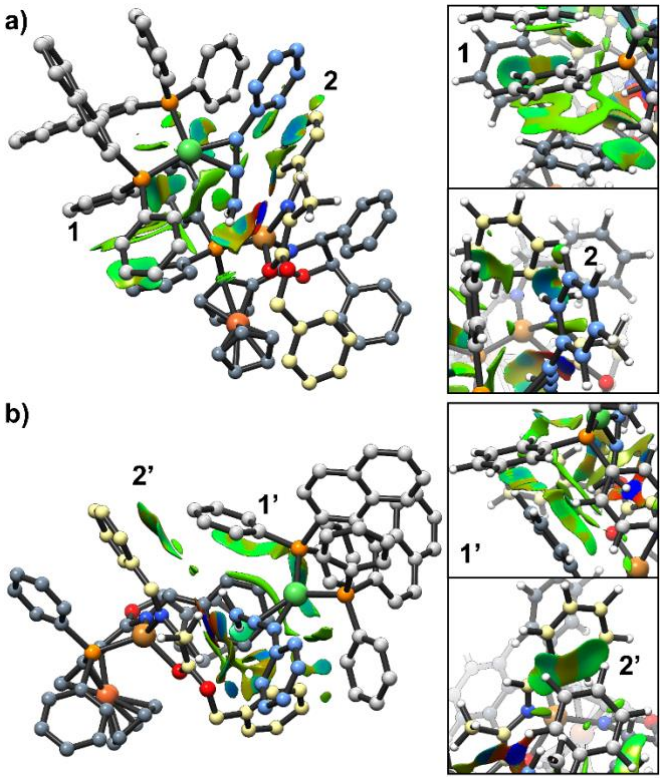

Fig. 3. DFT (B3LYP-D3 in CH_2Cl_2) structures of: a) pro-(*S*); and b) pro-(*R*) cooperative C-C coupling transition states, **TS$_{VI-VII}^C$**. Intermolecular NCIs surfaces computed by NCIPlot are also shown. NCIs interactions are represented as blue (strong), green (weak) and red (repulsive) blobs.

The selectivity is reverted when considering the *SS*-15-A isomer further supporting the central role of the inter-catalyst π–π stacking. Similar effects were recently reported by Sunoj and co-workers for the asymmetric coupling of azaaryl acetamide and cinnamyl methyl carbonate catalyzed by the Cu-Walphos and Ir-phosphoramidite cooperative system, [16] and by Houk, Dang and co-workers for the enantioselective Cu/Pd and stereodivergent Cu/Ir dual-catalytic syntheses of α,α-disubstituted amino acids.[33]

The nature of cooperativity in the full process was further assessed through calculation of the free energy profile involving both co-catalysts in a supramolecular aggregate from the beginning of the reaction. Our results, reported in Fig. S6 and S7, clearly show the energetic preference for the independent activation of the substrates by the separated co-catalysts. The aggregation in solution results in an endergonic step that ultimate leads to a barrier for the oxidative addition at nickel of 21.6 kcal mol^{-1}. These results indicate that direct cooperativity switches on only during the C-C coupling, while the formation of the electrophile and nucleophile moieties occurs in the separated Ni and Cu cycles, respectively. These results are in agreement with the recent mechanistic analysis by Mashima, Zhand and co-workers for the Cu/Ni cooperative formation of vicinal stereocenters.[21] The main features of our computed

catalytic mechanism are highlighted in Fig. 4. This is a Ni(0)/Ni(II) cycle in the nickel side, while Cu stays always as Cu(I). There is a direct connection between both cycles in the central point, with a bimetallic complex where the reductive elimination takes place. And there is a second connection between the two cycles through the $MeCO_2^-$ fragment, which is a side product from the Ni cycle but a necessary additive for the Cu cycle.

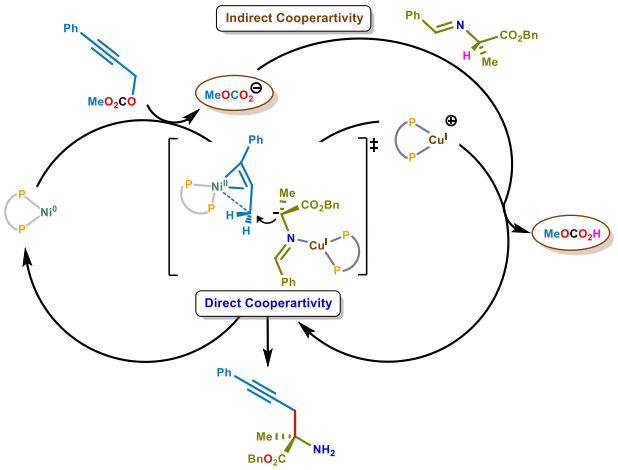

Fig. 4. Simplified Scheme of the computed catalytic cycle for activated co-catalysts $[Ni^0(\mathbf{L_1})(\mathbf{S_1})]$ and $[Cu^I(\mathbf{L_2})(\mathbf{S_2})]^+$. The cooperative steps are also highlighted.

In summary, we have characterized through DFT the mechanism of the asymmetric coupling of aldimine esters and propargylic carbonates catalyzed by the Ni-binap and Cu-phospherrox cooperative system. The activation of the substrates occurs independently in the separate metal complexes, which then cooperate in two different ways. There is a direct cooperativity where the two metal complexes get together to give rise to the enantioselective C-C coupling. And there is an indirect cooperativity through the transfer of a $MeCO_2^-$ unit from the Ni to the Cu cycle. This dual type of cooperativity had not been to our knowledge previously reported and highlights the possibilities of this type of processes.

Funding is acknowledged from CERCA Programme/Generalitat de Catalunya and Spanish MCIN/AEI (PID2020-112825RB-I00 and CEX2019-000925-S). GS thanks. Spanish MCIN Juan de la Cierva programme, FJC2019-029135-I.

Conflicts of interest

There are no conflicts to declare.

Notes and references

‡ Abbreviations: Binap = 2,2′-bis(diphenylphosphino)-1,1′-binaphthyl; Phospherrox = 1-[4,5-Dihydro-4-(1-methylethyl)-2-oxazolyl]-2-(diphenylphosphino)ferrocene.

§ Full computational details supplied in the ESI.† A data set collection of computational results is available in the ioChem-BD repository.[34]

1. S. Martínez, L. Veth, B. Lainer and P. Dydio, *ACS Catal.*, 2021, **11**, 3891-3915.
2. J. Campos, *Nature Reviews Chemistry*, 2020, **4**, 696-702.
3. U. B. Kim, D. J. Jung, H. J. Jeon, K. Rathwell and S.-g. Lee, *Chem. Rev.*, 2020, **120**, 13382-13433.
4. X. Huo, G. Li, X. Wang and W. Zhang, *Angew. Chem. Int. Ed.*, 2022, **61**, e202210086.
5. L. Wei and C.-J. Wang, *Chem Catalysis*, 2023, **3**, 100455.
6. F. Romiti, J. del Pozo, P. H. S. Paioti, S. A. Gonsales, X. Li, F. W. W. Hartrampf and A. H. Hoveyda, *J. Am. Chem. Soc.*, 2019, **141**, 17952-17961.
7. I. Funes-Ardoiz and F. Maseras, *Angew. Chem. Int. Ed.*, 2016, **55**, 2764-2767.
8. I. Funes-Ardoiz and F. Maseras, *ACS Catal.*, 2018, **8**, 1161-1172.
9. A. W. Jones, C. K. Rank, Y. Becker, C. Malchau, I. Funes-Ardoiz, F. Maseras and F. W. Patureau, *Chemistry - A European Journal*, 2018, **24**, 15178-15184.
10. O. Rivada-Wheelaghan, A. Comas-Vives, R. R. Fayzullin, A. Lledós and J. R. Khusnutdinova, *Chem. Eur. J.*, 2020, **26**, 12168-12179.
11. C. Wu, S. P. McCollom, Z. Zheng, J. Zhang, S.-C. Sha, M. Li, P. J. Walsh and N. C. Tomson, *ACS Catal.*, 2020, **10**, 7934-7944.
12. B. Bhaskararao, S. Singh, M. Anand, P. Verma, P. Prakash, A. C, S. Malakar, H. F. Schaefer and R. B. Sunoj, *Chem. Sci.*, 2020, **11**, 208-216.
13. M. Kalek and F. Himo, *J. Am. Chem. Soc.*, 2017, **139**, 10250-10266.
14. C. B. Musgrave, W. Zhu, N. Coutard, J. F. Ellena, D. A. Dickie, T. B. Gunnoe and W. A. Goddard, *ACS Catal.*, 2021, **11**, 5688-5702.
15. F. Zamani, R. Babaahmadi, B. F. Yates, M. G. Gardiner, A. Ariafard, S. G. Pyne and C. J. T. Hyland, *Angew. Chem. Int. Ed.*, 2019, **58**, 2114-2119.
16. A. Changotra, B. Bhaskararao, C. M. Hadad and R. B. Sunoj, *J. Am. Chem. Soc.*, 2020, **142**, 9612-9624.
17. C. Liu, C.-L. Ji, T. Zhou, X. Hong and M. Szostak, *Angew. Chem. Int. Ed.*, 2021, **60**, 10690-10699.
18. C. B. Musgrave, M. T. Bennett, J. F. Ellena, D. A. Dickie, T. B. Gunnoe and W. A. Goddard, *Organometallics*, 2022, **41**, 1988–2000.
19. G. Sciortino and F. Maseras, *Top. Catal.*, 2022, **65**, 105-117.
20. A. Matsuzawa, J. N. Harvey and F. Himo, *Top. Catal.*, 2022, **65**, 96-104.
21. J. Xia, T. Hirai, S. Katayama, H. Nagae, W. Zhang and K. Mashima, *ACS Catal.*, 2021, **11**, 6643-6655.
22. L. Wei, Q. Zhu, L. Xiao, H.-Y. Tao and C.-J. Wang, *Nat. Commun.*, 2019, **10**, 1594.
23. S. Li, Z. Wang, H. Xiao, Z. Bian and J. Wang, *Chem. Commun.*, 2020, **56**, 7573-7576.
24. L. Xiao, L. Wei and C.-J. Wang, *Angew. Chem. Int. Ed.*, 2021, **60**, 24930-24940.
25. X. Xu, L. Peng, X. Chang and C. Guo, *J. Am. Chem. Soc.*, 2021, **143**, 21048-21055.
26. L. Peng, Z. He, X. Xu and C. Guo, *Angew. Chem. Int. Ed.*, 2020, **59**, 14270-14274.
27. C.-H. Ding and X.-L. Hou, *Chem. Rev.*, 2011, **111**, 1914-1937.
28. Y. Peng, C. Han, Y. Luo, G. Li, X. Huo and W. Zhang, *Angew. Chem. Int. Ed.*, 2022, **61**, e202203448.
29. S. Kim, A. D. S. Richardson, A. Modak and N. J. Race, *J. Org. Chem.*, 2023, DOI: 10.1021/acs.joc.2c02254.
30. H. Yu, Q. Zhang and W. Zi, *Nat. Commun.*, 2022, **13**, 2470.
31. X.-X. Yan, Q. Peng, Y. Zhang, K. Zhang, W. Hong, X.-L. Hou and Y.-D. Wu, *Angew. Chem. Int. Ed.*, 2006, **45**, 1979-1983.
32. J. Contreras-García, E. R. Johnson, S. Keinan, R. Chaudret, J.-P. Piquemal, D. N. Beratan and W. Yang, *J. Chem. Theory Comput.*, 2011, **7**, 625-632.
33. B. Li, H. Xu, Y. Dang and K. N. Houk, *J. Am. Chem. Soc.*, 2022, **144**, 1971-1985.
34. M. Álvarez-Moreno, C. de Graaf, N. López, F. Maseras, J. M. Poblet and C. Bo, *J. Chem. Inf. Model.*, 2015, **55**, 95-103.

